Dense avalanche numerical modeling Interaction between avalanche and structures

Mohamed Naaim
Snow and avalanches control – ETNA/Cemagref
BP : 76 Domaine universitaire
F-38402 Saint Martin d'Hères

ABSTRACT: Applications of the Saint Venant equations were extended to rapid gravity flows of geophysical fluid with a non-newtonian behavior such as snow avalanches. This paper presents a numerical and physical approach for snow avalanches considered as a granular material. The mathematical equation system is numerically solved. In order to validate the numerical modeling, a reduced scale model is built. The materials are retained behind a dam by a rapid opening gate. The downhill slope is divided into two sections: a steep slope with a channeled flowing zone and a section with an abrupt widening with a slope angle of zero degree. Several experiments have been done with various volumes of different materials. The following parameters were measured in each experiment: 1) the evolution of the height and the forces in three locations along the flowing zone, 2) the velocity field at the surface of the avalanche, and 3) the mapping of the deposition zone. The whole experiments have been numerically reproduced. Engineers in charge of the protection against dense avalanches, increasingly recommend the construction of protection devices whose function, at the end of the flow zone, is to dissipate the avalanche energy. The last section of this paper deals with an attempt of efficiency evaluation of these structures using numerical modeling.

1. INTRODUCTION

In winter and in mountain regions, one often observes two kind of snow avalanches: dense avalanches and powder avalanches. Earlier studies approached the totality of these flows by a theory issued from hydraulics [Vollemy 1955]. In recent studies, the two type of flows are approached by two different theories. The study of powder avalanche flow is based on the analogy with the density current. The powder avalanche (air + snow particles) is considered as a Newtonian fluid and its flow is turbulent [Naaim, 1997]. On the other hand, dense flows, without aerosol, have been assimilated to a continuous material with a non-newtonian behavior, to which laws issued from fluid mechanics are applied.

The dense avalanche is composed of snow particles with different forms and dimensions. It contains snow blocks and snow spheres. The snow metamorphosis produces different kind of cohesion. One can also find some water as interstitial fluid that strongly modifies the structure and behavior of the snow.

The assimilation of the snow flow to a granular material flow knocks to several reserves that are modification of the material structure and particle form during the flow and the appearance of the water by snow fusion due to friction and energy dissipation in heat. For snow in very cold weather, it appears reasonable to assimilate the moving snow to a granular material. However, this assimilation becomes disputable when the snow is humid. In humid snow flow, one observes the formation of spheres with various dimensions.

In this paper's framework, we only consider the ideal case of a cold and dry snow composed exclusively of snow grain. Its assimilation to a dry granular material is more well off in this case. The case of flows of dry granular materials has for a long time been the objective of researches in terms of rheology. Since the pioneer works of [Bagnold, 1954], several theoretical researches have dealt with behavior laws of material flows, such as works of Haff (1983), and Savage and Hutter (1989).

Haff (1983) has described the limits of the assimilation of a granular material to a simple fluid. Important differences exist between the grains and the molecules. A grain of sand is 10^{18} times heavier and more voluminous than a water molecule. The interaction between molecules is completely elastic while the grain interactions can be made by shocking and friction, and it is always accompanied by energy loss. The poorly sorted granulometry, the irregular form of grains, and the fact that grain shocks are not always centered will create new difficulties that the theory has to take into account for the establishment of behavior laws for granular materials.

Dense flows are characterized, by the fact that a very weak distance compared to the average grain diameter separates neighboring grain surfaces, which results in a weak air incorporation during the flow. The dilatation of the initial volume is therefore considered to be weak and the porosity of such material does not evolve during its flow.

The grains mass conservation is: $\frac{\partial \rho}{\partial t} + \mathrm{div}(\rho \vec{u}) = 0$

For a "simple" fluid (Newtonian), the equation of the momentum conservation contains a viscous force term, that is proportional to the velocity gradient. The proportionality coefficient, called dynamic viscosity, is a physical characteristic of the fluid. For a granular fluid, a similar viscosity can be constructed. But, it is a more complex function than in the case of a Newtonian fluid. We can find in the literature several behavior laws that differ in the function connecting to the velocity gradient.

The main existing behavior laws for a planar flow are the Bingham model: $\tau = \tau_c + \mu \frac{\partial u}{\partial y}$, the Bagnold model: $\tau = \mu (\frac{\partial u}{\partial y})^2$; and the Mohr-Coulomb model: $\tau = -\rho g h \cos(\theta) \tan(\varphi)$.

The last one was proposed and used by Savage and Hutter (1989). The friction between the ground and the flowing material produces the momentum dissipation.

By analogy with a Newtonian fluid, conservation of the momentum for a granular fluid can be written as:

$$\frac{\partial \rho u_i}{\partial t} + \mathrm{div}(\rho u_i . \vec{u}) + \frac{\partial p}{\partial x_i} = \rho \vec{g} . x_i + \tau_{ji,j}$$

Where p is the pressure, g the gravity coefficient, τ_{ij} the stress tensor and $\vec{x}_i$ the base system of the axis (Oxyz) in which Oxy stands for the horizontal plane and Oz stands for the up-ward vertical axis.

2. NUMERICAL MODELING

In order to study the dense flows we choose a model from Hydraulics. In this case, the velocity vector ($\vec{u}$) is replaced by its vertical average ($\vec{\bar{u}}$). Equations describing the flow are obtained by integrating vertically the mass and the momentum conservation taking into account the following hypotheses

- The flow is made of snow particles and the momentum dissipation results from the friction at the ground surface interface, and from grain shocks.
- The vertical pressure distribution is hydrostatic.

This allows neglecting the internal dissipation and makes the vertical integration easier. We obtain the following equation system :

$$\frac{\partial h}{\partial t} + \frac{\partial h\bar{u}}{\partial x} + \frac{\partial h\bar{v}}{\partial x} = 0$$

$$\frac{\partial (h \vec{\bar{u}})}{\partial t} + \frac{\partial}{\partial x}\begin{pmatrix} h\bar{u}^2 \\ h\bar{u}\bar{v} \end{pmatrix} + \frac{\partial}{\partial y}\begin{pmatrix} h\bar{u}\bar{v} \\ h\bar{v}^2 \end{pmatrix} + \vec{\nabla}(kg\cos(\theta)\frac{h^2}{2})$$

$$= hg\begin{pmatrix} \sin(\theta_x) \\ \sin(\theta_y) \end{pmatrix} - gh\cos(\theta)\tan(\phi)\,\vec{\bar{u}}/\|\vec{\bar{u}}\| - \mu\left[\frac{\partial \vec{u}}{\partial y}\right]^2$$

Where h is the flow height, θ_x and θ_y are the slopes in x and y directions and θ is the total terrain slope.

So, in order to study the flow of dense snow avalanches on a given site, we need to access its topography. We have chosen to process it under the form of a digital terrain model, which is composed of a triangular irregular network. On each element of the mesh the equations between two different times are integrated. Let T_h a topology of the space formed by all the elements. For each element K_i of T_h, we denote Γ_i its contour, A_i its surface and Γ_{ij} its common contour with K_j. We have solved the system of equations in finite volumes by a Godunov numerical scheme, which is second order in space and in time.

2.1 Numerical scheme

We begin by defining a spatial average of U = (h,hu,hv) on each element K_i in time t^n and t^{n+1} by the projection:

$$U_{ki}^n = \frac{1}{V_{ki\,ki}} \int U(\vec{x}, t^n) dv \text{ and}$$

$$U_{ki}^{n+1} = \frac{1}{V_{ki\,ki}} \int U(\vec{x}, t^{n+1}) dv$$

The numerical solution is then made by integration of the equations system on [Ki] x [t^n, t^{n+1}], we obtain the following numerical scheme:

$$U_{ki}^{n+1} = U_{ki}^n - \frac{\Delta t}{S_{ki}} \sum_1^{na} \begin{bmatrix} E \\ F \end{bmatrix}^{\rightarrow} n\, l_a + \Delta t . G(\frac{U_{ki}^n + U_{ki}^{n+1}}{2})$$

Where G is contribution of the second member and na is the number of neighboring edges of K_i. We determine the numerical flux through each edge using simplified Riemann solver [Naaim, 1991].

The gradient are calculated by minimizing the function F:

$$F = \sum_{j=1}^{nev} \left(\left[U_{kj} - U_{ki} - \begin{bmatrix} \partial U/\partial x \\ \partial U/\partial y \end{bmatrix} (\vec{x}_{kj} - \vec{x}_{ki}) \right]^2 \right)$$

Where nev is the number of neighbors of Ki. These gradients are then limited in order to avoid the creation of new extremum. The Riemann problem is written as:

$$\frac{\partial U}{\partial t} + \frac{\partial}{\partial x_n}\begin{bmatrix} E \\ F \end{bmatrix} = 0 / \begin{cases} U = U_{kg} + \begin{bmatrix} Ux_{kg} \\ Uy_{kg} \end{bmatrix} (\vec{x}_a - \vec{x}_{kg}) \text{ if } x_n < 0 \\ U = U_{kd} + \begin{bmatrix} Ux_{kd} \\ Uy_{kd} \end{bmatrix} (\vec{x}_a - \vec{x}_{kd}) \text{ if } x_n > 0 \end{cases}$$

Where a is indication of neighbor facet of the element.

After the numerical flux calculation, the contribution of source terms (second member terms) is explicitly calculated and added to the final solution.

3. SCALE MODEL

In order to validate our numerical modeling, we have build and implemented a scale model.

3.1 Dimensionless equations

The governing equations are written in dimensionless form using h_o and u_o respectively as a length and velocity scales:

$$\frac{\partial(h\vec{\bar{u}})}{\partial t}+\frac{\partial}{\partial x}\begin{pmatrix} h\bar{u}^2 \\ h\overline{uv}\end{pmatrix}+\frac{\partial}{\partial y}\begin{pmatrix} h\overline{uv} \\ h\bar{v}^2\end{pmatrix}+\vec{\nabla}(kg\cos(\theta)\frac{h^2}{2})$$

$$=\frac{1}{F_r}\left(\begin{pmatrix}\sin(\theta_x)\\ \sin(\theta_y)\end{pmatrix}-\cos(\theta)\tan(\phi)\,\vec{\bar{u}}/\|\vec{\bar{u}}\|\right)-\mu\left[\frac{\partial\vec{u}}{\partial y}\right]^2$$

The classical Froude number expresses the dynamic similarity by:

$$F_r=\frac{u_o}{\sqrt{gh_o}}.$$

3.2 Scale model

The scale model is composed of three parts. The first part is a reservoir where the material is initially stored. A gate ends this reservoir and it can be quickly opened. In this case, we can simulate the instantaneous release of the avalanche. The second part of the model is a canalized flowing zone with a high slope angle. The last part is the horizontal run-out zone characterized by a brusque widening. For each experimental material, the surface of scale model was covered by plastic cloth in order to have a friction angle between the material and the scale model equal to the internal friction angle.
The geometric scale of our model compared to a real avalanche path is not easy to define. In the scale model, the vertical distance covered by the avalanche is about 2 m. In nature, the vertical distance covered by avalanches varies between 200 m and 1000 m. This means that our geometric scale varies between 1/50 and 1/500.

3.3 Measurements devices

Three materials were used: sand, gravel and PVC balls. Several experiments were realized using different initial volumes. For each experiment the following measurements were done:

- the evolution of the height versus time in three locations along the flowing zone. Three sensors were placed at 50-cm, 110-cm and 130-cm from the gate. These sensors allowed us measuring the height of the flow. The frequency of these sensors is 100 Hertz. The measurements are very accurate but the irregularities of the materials induce an error of about 3.10^{-3}-m.
- The evolution of the tangential and the normal forces exerted by the flow on the flowing zone surface. By doing this, we were able to confirm the behavior of the flowing material and to determine the real (dynamic) friction angle.
- Once the flow stopped in the run-out zone, the device consisting of two ultra-sonic sensors allowed us measuring and mapping the deposit. This was done by measuring in a grid of 5-cm edge, the height of the deposit.
- The velocity of the granular material flow is obtained by a camera and image processing system. Colored particles were placed initially in the starting zone and their movements are recorded and analyzed by the image processing system.

Characteristics of the experimental materials are reported in the following table.
Table 1 :

	Mean diameter (m)	Density ($kg.m^{-3}$)	φ (°)
Gravel	$2.5\ 10^{-3}$	1500	35.5
Sand	$1.8\ 10^{-4}$	1380	32.5
Balls of PVC	$1.2\ 10^{-4}$	600	29

Where φ is the friction angle. All these materials were dry and their granulometry curves were very narrow.

4. COMPARISON BETWEEN THE NUMERICAL AND EXPERIMENTAL RESULTS

In this section, the objective was to compare the numerical model with the experimental results. Through this comparison, we analyzed the role of different factors influencing the flow of such granular material. The main factors influencing the flow are the initial volume, the slope angle of the flowing zone and the friction angle between the material and the ground.
This analysis allowed us quantifying the importance of these factors and demonstrating the model ability to reproduce the experimental results in the flowing zone and the run-out zone.

4.1 Forces measurements :

Using the force and height measurements, we were able to determine the friction angle and to show that the Mohr-Coulomb model is valid for this kind of flow.

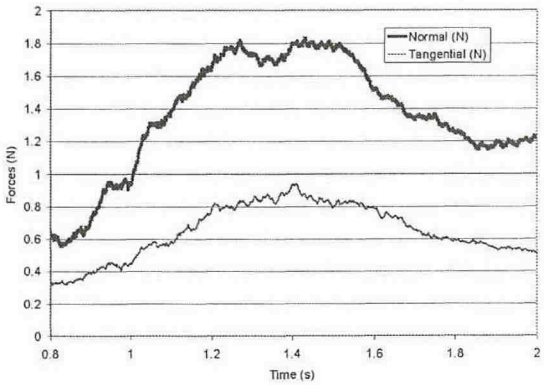

Figure 1: Force measurements

4.2 Flow phase

The flowing zone corresponds to the zone located between the gate and the brusque widening. In this zone we studied the roles played by the initial volume, the slope angle and the friction coefficient. For the three materials, we studied three slope angles and three initial volumes.

4.2.1 Volume

In order to illustrate the initial volume importance, we present here the results obtained using a slope angle of 45° and the gravel material. We realize three experiments using three different volumes V1, V2 and V3 corresponding to 20 kg, 30 kg and 40 kg. The numerical and experimental results are displayed in figure 2. This figure shows that the height increases with the initial volume. The front velocity

represented in this figure by the arriving time increases also according to the initial volume.

Taking into account the measurements accuracy, we concluded that the numerical results are close to the experimental ones and that the numerical model can reproduce well the experimental initial volume effect.

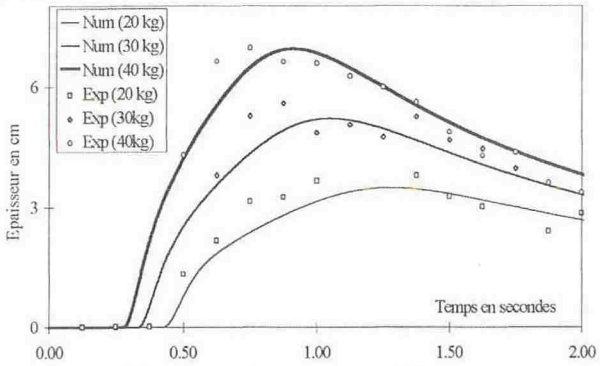

Figure 2: initial volume Influence

4.2.2 Friction angle effect

In order to illustrate the importance of the friction angle, we numerically and experimentally studied two different materials, the gravel and the PVC balls.

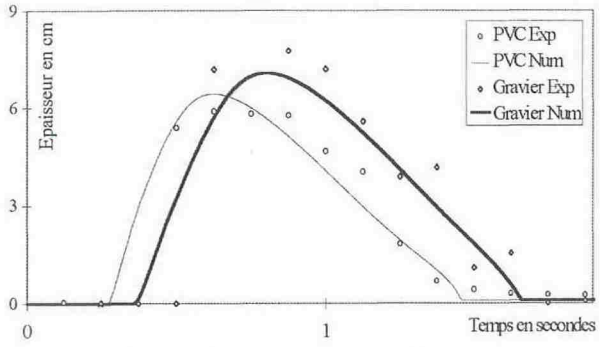

Figure 3 : friction angle influence

Figure 3, in which the results obtained for a slope angle equal to 60° are displayed, shows that a small variation of the friction angle induce important change of the maximum height of the flow. Comparing the numerical results with the experimental results we conclude that the numerical model can reproduce the experimental results well.

4.2.3 Slope angle effect

In order to illustrate the importance of the slope angle we present two cases using the same material and two different slope angles: 40° et 60°. Figure 4 shows the comparison between the experimental and the numerical results in the case of gravel material with an initial volume corresponding to 30 kg. From this figure, we can conclude that the slope is very important because the front velocity and maximum height are very sensitive to it. We can also observe that the numerical model results are very close to the experimental ones.

4.3 Phase of deposit

In order to illustrate the numerical model ability to reproduce geometry of the deposit we present the case of gravel material with a slope angle of 45° and an initial volume corresponding to 30 kg. For this case, the result is presented in figures 5 and 6 under two profiles: profile along the deposit and profile transverse to the deposit. The profile along deposit is realized in the axis of the flowing zone and the transverse deposit profile is realized orthogonaly to this axis.

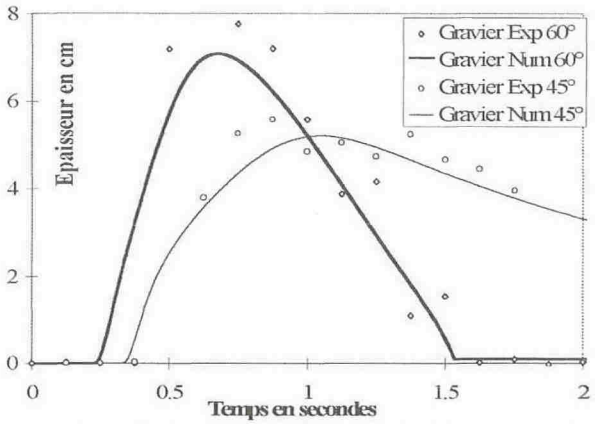

Figure 4: slope angle effect

Through these two profiles, we can show that the model can reproduce the deposit geometry very well.

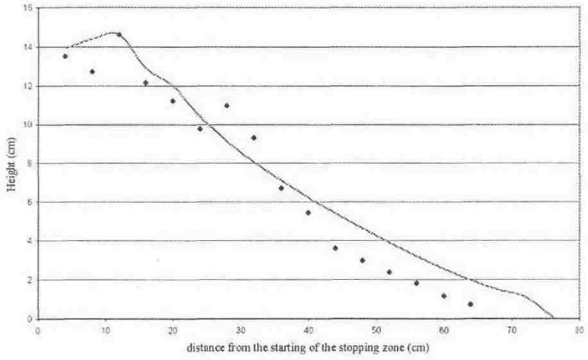

Figure 5: Profile example along the deposit (comparison numerical-- /experimental results ♦)

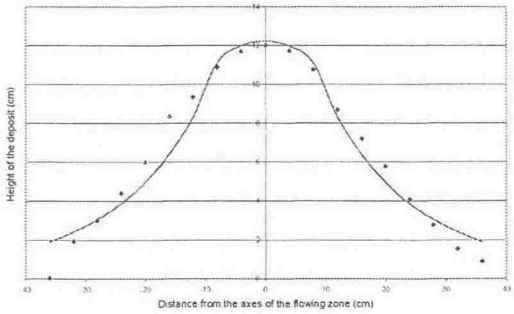

Figure 6: Example of the transverse deposit profile (comparison numerical-- /experimental results♦)

The numerical model reproduced all experimental observations. It is very important to notice the importance of the initial volume, the slope angle and the friction angle. This remark shows that these parameters have to be estimated very carefully when applying these kind of models to real cases.

5. EFFICIENCY OF DISSIPATION STRUCTURE :

Engineers in charge of the protection against dense avalanches, increasingly recommend the construction of protection devices which function, at the end of the flowing zone, is to dissipate the energy of the avalanche. The

objective here is to determine the reduction in terms of dynamic pressure of this structure. That is why we used the numerical model. The studied device is presented in figure 7.

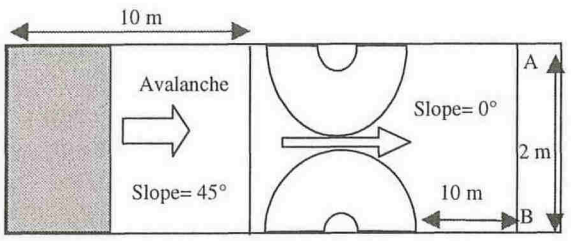

Figure 7: device used in numerical experiments

We introduce as initial condition, an avalanche with the height h, the friction angle of 30° and μ=0.01. The obstacle is conic determined by its height (d) and its surface diameter near the ground (2l).

In AB section, we determine the pressure coefficient reduction comparing the result obtained with the obstacle to the one obtained without the obstacle. The pressure reduction coefficient is defined as:

$$\alpha = \frac{\text{Max}\left(\int_{AB,d=0} \frac{1}{2}\rho h\bar{u}^2 ds - \int_{AB,d=1} \frac{1}{2}\rho h\bar{u}^2 ds \right)}{\max\left(\int_{AB,d=0} \frac{1}{2}\rho h\bar{u}^2 ds \right)}$$

Using the same device, we determined the coefficient α for the following avalanche heights 1m, 2m, 3m and 4m.

In the case of h=1 m, and with the obstacle presence, the avalanche stopped before getting to the line AB. In this case α is taken to be equal to 1. For h=2m, h=3m and h=4m the coefficient α is calculated and presented in figure 10.

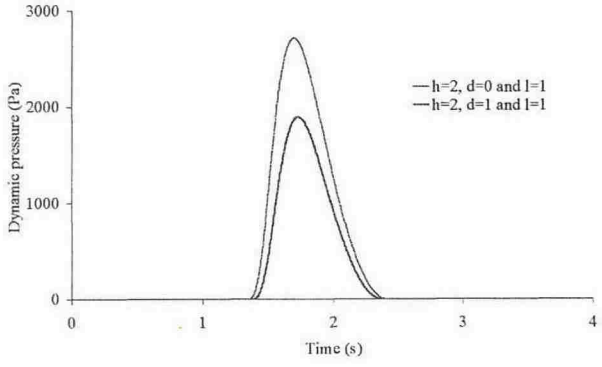

Figure 8: Avalanche with h=2 m

We observe through these results that the structure is more efficient if the dimension of avalanche is close to the dimension of the structure. With the obstacle the avalanche stopped before AB section. The reduction of the dynamic pressure of the avalanche is 100%. If the avalanche height is twice the structure height, the reduction of the dynamic pressure is 30 %. If the height is three or four times the structure dimension, the reduction is smaller than 16% and 11% respectively. α is approximated by: $\alpha = 0.96[h/d]^{-1.58}$

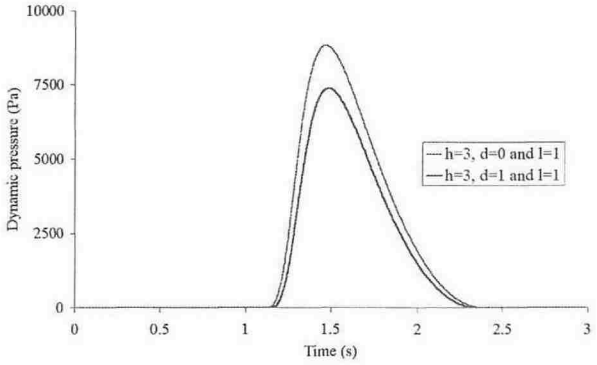

Figure 9: Avalanche with h=3 m

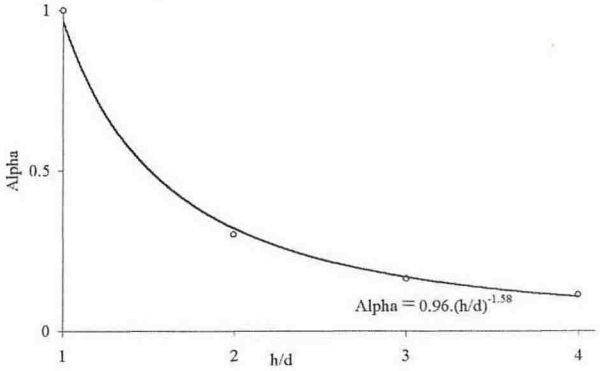

Figure 10: Dynamic pressure coefficient reduction

6. CONCLUSIONS :

A numerical model based on Saint Venant equations was built to study the flow of a dry avalanches. The behavior law is a granular material one. In order to validate the numerical modeling, a reduced scale model is built. Several experiments allowed us to validate the model. Engineers in charge of the protection against dense avalanches, increasingly recommend the construction of protection devices which function, at the end of the flow zone, is to dissipate the energy of the avalanche. The last section of this paper deals with an attempt of efficiency evaluation for these structures using numerical modeling. The reducing effect is optimal when the obstacle dimension is close to the avalanche one.

REFERENCES :

Bagnold, R.A., 1956,"The flow of cohesionless grains in fluids" Proc. R. Soc. Lond. A249, 235-297.

Haff, P.K., 1993, "Grain flow as a fluid-mechanical phenomenon", *J. Fluid. Mech.*, **134**, 401-430.

Naaim,M., 1995, "Modélisation numérique des avlanches aérosols", *La Houille Blanche*, **N°5**, 56-62

Savage, S.B., Hutter, K, 1989, "The motion of a finite mass of granular material down a rough incline", *J. Fluid. Mech.*, **199**, 177-215.

Vollemy, A., 1955," Uber die Zerstoreungskraft von Lawinen, Schweizerische Bauzeitung, **73**, 159-165.